Dalton Transactions

ROYAL SOCIETY OF CHEMISTRY

PAPER

View Article Online
View Journal

Cite this: DOI: 10.1039/d4dt00280f

Tandem templating strategies facilitate the assembly of calix[8]arene-supported Ln_{18} clusters†

Yushu Jiao, [a] Sergio Sanz, *[b] Jan van Leusen, [a] David Gracia,[c] Angelos B. Canaj, [d] Marco Evangelisti, *[c] Euan K. Brechin, *[d] Scott J. Dalgarno *[e] and Paul Kögerler *[a,b]

Received 30th January 2024,
Accepted 31st January 2024

DOI: 10.1039/d4dt00280f

rsc.li/dalton

Calix[*n*]arenes offer ideal chemical functionality through the polyphenolic lower rim to construct nano-sized coordination clusters with lanthanide (Ln) metal ions (*e.g.*, Nd^{III}_{10}, Gd^{III}_{8}). However, the number of metal centers they can accommodate is still limited compared to that achievable with smaller ligands (*e.g.*, Gd^{III}_{140}, Gd^{III}_{104}). Here, we exploit a combination of the "anion template strategy" and "templating ligands" to synthesise three highly symmetric (D_{3h}, trigonal planar) Ln^{III}_{18} (Ln = La, Nd, and Gd) systems, representing the largest calix[*n*]arene-based coordination clusters yet. The Ln^{III}_{18} fragment is templated by a chloride anion located at the center of the cluster, wherefrom twelve μ_3-OH^- ligands bind 'internally' to the eighteen Ln^{III} ions. 'Externally' the metallic skeleton is connected by *p-tert*-butylcalix[8]arene, oxo, chloro and carbonate ligands. The crystal packing in the lattice reveals large cylindrical channels of ~26 Å in diameter, whose pore volume corresponds to ~50% of the unit cell volume (using a 1.2 Å spherical probe radius). Magnetic measurements reveal the predominance of weak antiferromagnetic exchange in the Gd analog. Heat capacity data of Gd^{III}_{18} reveal a high magnetic entropy with $-\Delta S_m$ = 23.7 J K^{-1} kg^{-1}, indicating potential for engineering magnetic refrigerant materials with calix[8]arenes.

Introduction

The synthesis of high nuclearity, homometallic lanthanide (Ln) coordination clusters has been developed in recent decades owing to their fascinating topological configurations and unique chemical and physical properties, with potential applications in fields as diverse as catalysis, optics, and magnetism.[1] The synthesis of such clusters entails ligands that are able to define the outer sphere of the molecule by limiting the uncontrollable hydrolysis of the metal ions. The latter is characterized by the production of intractable precipitates of metal hydroxides and/or oxohydroxides. Several classes of ligands have been successfully tested for this purpose, producing giant homometallic Ln clusters including Gd^{III}_{140},[1a] Ln^{III}_{104},[1b] Dy^{III}_{76},[1c] Dy^{III}_{72},[1d] Ln^{III}_{60},[1e,f] and Ln^{III}_{48},[2] whose metallic cores are commonly constructed by the repetition of a small number of well-defined building blocks constructed from metal-hydroxo motifs. These include triangular $\{Ln_3(\mu_3\text{-OH})\}$, tetrahedral $\{Ln_4(\mu_3\text{-OH})_4\}$ and trigonal bipyramidal $\{Ln_5(\mu_3\text{-OH})_6\}$. The metallic skeletons of these clusters therefore tend to conform to specific polyhedra possessing the same characteristic symmetries as their building blocks (*e.g.*, tetrahedral T_d, cubic O_h, dodecahedron I_h, *etc.*).[3]

Perhaps the most successful calix[*n*]arene ligands in the design and construction of high-nuclearity metal coordination clusters are the *p-tert*-butylcalix[*n*]arenes (H_nTBC[*n*]) comprising either 4 or 8 phenolic units (H_4TBC[4] and H_8TBC[8]). Although both have been commonly employed in supramolecular chemistry (3331 and 161 hits in the Cambridge Structural Database, CSD, respectively), their use as coordination ligands to build homometallic Ln clusters remains relatively underexplored (16 and 15 hits in the CSD for H_4TBC[4] and H_8TBC[8], respectively). The vast majority are dimeric Ln_2 species, particularly for *p-tert*-butylcalix[8]arene. Examples of larger nuclearity cages include $[Nd^{III}_{10}(TBC[8])_2]$, $[Gd^{III}_{8}(TBC[8])_2]$, $[Dy^{III}_{7}(TBC[8])_2]$, and $[Tb^{III}_{6}(TBC[4])_2]$.[4]

[a]*Institute of Inorganic Chemistry, RWTH Aachen University, 52056 Aachen, Germany. E-mail: paul.koegerler@ac.rwth-aachen.de*
[b]*Peter Grünberg Institute, Electronic Properties (PGI-6), Forschungszentrum Jülich, 52425 Jülich, Germany. E-mail: s.calvo@fz-juelich.de*
[c]*Instituto de Nanociencia y Materiales de Aragón (INMA), CSIC – Universidad de Zaragoza, Departamento de Física de la Materia Condensada, 50009 Zaragoza, Spain. E-mail: evange@unizar.es*
[d]*EaStCHEM School of Chemistry, The University of Edinburgh, David Brewster Road, Edinburgh, EH9 3FJ, UK. E-mail: ebrechin@ed.ac.uk*
[e]*Institute of Chemical Sciences, Heriot-Watt University, Riccarton, Edinburgh, EH14 4AS, UK. E-mail: S.J.Dalgarno@hw.ac.uk*

†Electronic supplementary information (ESI) available. CCDC 2299004. For ESI and crystallographic data in CIF or other electronic format see DOI: https://doi.org/10.1039/d4dt00280f

The synthesis of polynuclear coordination clusters with a particular blend of physical properties has resulted in magnetic molecules that can potentially be employed as efficient cryogenic magnetic refrigerants *via* the magnetocaloric effect (MCE).[5] Magnetic entropy (ΔS_m) and adiabatic temperature (ΔT_{ad}) changes take place in a magnetocaloric material following the change of an applied magnetic field (ΔB). The ideal metal ion to exploit is Gd^{III} due to its large isotropic spin $s = 7/2$, leading to several high-nuclearity coordination clusters that possess large molecular magnetic entropies at low temperatures.[6] Such species are energy-efficient alternatives to traditional cooling materials such as ^3He or ^4He.[7]

We have recently focused at a breadth of different synthetic conditions in calix[*n*]arene coordination chemistry, including the implementation of the "anion template strategy" and the utilization of "templating ligands". The former has long proven adept in constructing high-nuclearity clusters with a range of organic ligands, but strangely has been almost neglected in calix[*n*]arene coordination chemistry. The introduction of "templating ligands" – critical for the molecule's formation but not integrated into its structure – is believed to play a crucial role in directing the self-assembly of large nuclearity species by isolating the smaller building blocks, preventing rapid aggregation into smaller complexes with more stable topologies. The recent successful synthesis of the molecular iron oxides Fe^{III}_{34} and Fe^{III}_{30},[8] achieved using this methodology, provides an excellent demonstration of its potential and relevance to be introduced in the field of calixarene chemistry.

Here we adopt these strategies in the synthesis of three highly symmetric (D_{3h}, trigonal planar) Ln^{III}_{18} clusters of formula $[Ln^{III}_{18}(TBC[8])_3(\mu_4\text{-}O)_3(\mu_3\text{-}Cl)_6(\mu_3\text{-}OH)_{12}(\mu_3\text{-}CO_3)_2(H_2O)_6(DMF)_{18}Cl]OH{\cdot}H_2O{\cdot}12DMF$, representing the largest known calix[*n*]arene-based coordination clusters.

Experimental section

Synthetic procedure

All solvents and reagents (99.9%) used in this work were obtained from commercial sources. $[Ln^{III}_2(H_2TBC[8])(DMSO)_3(H_2O)]{\cdot}2H_2O{\cdot}3DMSO$ was synthesized according to a modified literature[9] method as described below.

Preparation of $[Ln^{III}_2(H_2TBC[8])(DMSO)_3(H_2O)]{\cdot}2H_2O{\cdot}3DMSO$ (Ln_2)

A mixture of $H_8TBC[8]$ (150 mg, 0.115 mmol), $Ln^{III}Cl_3{\cdot}6H_2O$ (132.51 mg for $La^{III}Cl_3{\cdot}6H_2O$, 134.50 mg for $Nd^{III}Cl_3{\cdot}6H_2O$, and 139.38 mg for $Gd^{III}Cl_3{\cdot}6H_2O$; 0.375 mmol) in 14 mL DMSO/MeCN (v : v = 1 : 1) was stirred for 5 min and then triethylamine (0.18 mL, 1.29 mmol) was added. The solution was further stirred for another 2 h. The resulting solution was left to stand at room temperature overnight to allow the formation of a white precipitate. The crude product was then isolated by filtration and purified by slow diffusion of *tert*-butyl methyl ether into a $CHCl_3$ solution of the product affording colorless needle-shape crystals of $[Ln^{III}_2(H_2TBC[8])(DMSO)_3(H_2O)]{\cdot}2H_2O{\cdot}3DMSO$.

Synthesis of $[La^{III}_{18}(TBC[8])_3(\mu_4\text{-}O)_3(\mu_3\text{-}Cl)_6(\mu_3\text{-}OH)_{12}(\mu_3\text{-}CO_3)_2(H_2O)_6(DMF)_{18}Cl]OH{\cdot}H_2O{\cdot}12DMF$ (1)

A solution of La_2 (314.45 mg, 0.15 mmol) and 1,3,5-tricarboxylic acid (15.75 mg, 0.075 mmol) in 8 mL $CHCl_3$/DMF/MeOH (v : v : v = 3 : 3 : 2) was stirred for 5 min. Afterwards, NBu_4OH (0.1 mL, 40% in water) was slowly added to the solution under stirring and left to stir for 1 hour. The resulting mixture was then sealed in a PTFE-lined bomb and heated to 120 °C for 48 h. After cooling slowly to room temperature, the cloudy solution was filtered to yield a clear yellow solution. Brown, block-shaped crystals were obtained by slow diffusion of hexane into the mother liquor over a period of four weeks. Yield (5 mg, 3.6%). IR ($\tilde{\nu}/cm^{-1}$): 2953 (m), 2903 (w), 2867 (w), 1653 (vs), 1598 (w), 1453 (s), 1390 (m), 1360 (m), 1297 (m), 1267 (m), 1207 (s), 1108 (w), 1023 (m), 907 (w), 862 (w), 818 (m), 804 (w), 739 (m), 679 (m), 606 (w). **Crystal data (CCDC 2299004):** $C_{356}H_{549}Cl_7La_{18}N_{30}O_{83}$, M = 9325.75 g mol^{-1}, trigonal, space group $P\bar{3}1c$ (no. 163), a = 32.5846(4) Å, c = 34.4461(6) Å, V = 31 673.5(10) Å^3, Z = 2, T = 100(2) K, μ(CuKα) = 9.799 mm^{-1}, D_{calc} = 0.978 g cm^{-3}, 458 160 reflections measured ($6.264° \leq 2\theta \leq 130.688°$), 18 091 unique ($R_{int}$ = 0.1166, R_{sigma} = 0.0431) which were used in all calculations. The final R_1 was 0.0832 ($I > 2\sigma(I)$) and wR_2 was 0.3071 (all data).

Synthesis of $[Nd^{III}_{18}(TBC[8])_3(\mu_4\text{-}O)_3(\mu_3\text{-}Cl)_6(\mu_3\text{-}OH)_{12}(\mu_3\text{-}CO_3)_2(H_2O)_6(DMF)_{18}Cl]OH{\cdot}H_2O{\cdot}12DMF$ (2)

Compound **2** was prepared using the same synthetic procedure as compound **1**, with the substitution of La_2 for Nd_2 (134.50 mg, 0.375 mmol). The reaction yielded 6 mg (4.2%) of dark-green block-like crystals. IR ($\tilde{\nu}/cm^{-1}$): 2951 (m), 2903 (w), 2863 (w), 1653 (vs), 1605 (w), 1460 (s), 1390 (m), 1360 (m), 1296 (m), 1267 (m), 1206 (s), 1107 (w), 1023 (w), 905 (w), 867 (w), 818 (m), 802 (w), 738 (m), 678 (m), 605 (w).

Synthesis of $[Gd^{III}_{18}(TBC[8])_3(\mu_4\text{-}O)_3(\mu_3\text{-}Cl)_6(\mu_3\text{-}OH)_{12}(\mu_3\text{-}CO_3)_2(H_2O)_6(DMF)_{18}Cl]OH{\cdot}H_2O{\cdot}12DMF$ (3)

Compound **3** was prepared using the same synthetic procedure as compound **1**, replacing La_2 with Gd_2 (139.38 mg, 0.375 mmol) and adjusting the temperature from 120 to 150 °C for 24 h. Brown block-like crystals were obtained by slow evaporation of the mother liquor over four weeks. Yield (4 mg, 2.7%). IR ($\tilde{\nu}/cm^{-1}$): 2953 (m), 2905 (w), 2865 (w), 1655 (vs), 1611 (w), 1469 (s), 1390 (m), 1360 (m), 1299 (m), 1266 (m), 1207 (s), 1110 (w), 1025 (w), 908 (w), 864 (w), 819 (m), 806 (w), 741 (m), 682 (m), 606 (w).

Crystal structure information

A single crystal of **1** was selected and measured on a Bruker D8 Venture diffractometer operating with Cu–Kα radiation (λ = 1.54178) at 100(2) K. Using Olex2,[10] the structure was solved with the SHELXT[12] structure solution program using Intrinsic Phasing and refined with the SHELXL[11] refinement package using Least Squares minimization. There is a considerable amount of disorder present in the structure, which is not

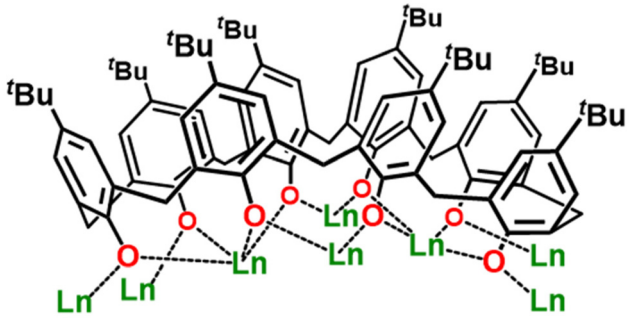

Fig. 1 Representation of *p-tert*-butylcalix[8]arene (TBC[8]) and its coordination abilities presented in Ln^{III}_{18}. The ligand is in a twofold double-cone conformation, adopting a μ_2-O binding mode in each phenoxide unit toward the Ln ions.

uncommon for one of this nature, particularly when channels are formed by pseudo-spherical assemblies that necessarily pack to form solvent-occupied channels or regions in the crystal lattice. A number of the upper-rim ^{t}Bu groups of the calix[8]arene are disordered and have been modeled at partial occupancies. The hydroxide counterion and waters of crystallization were also handled in this way, whilst co-crystallized DMF was dealt with *via* the use of a solvent mask as it could not be modeled effectively. Given the level of disorder it was necessary to employ numerous restraints, but considering the severity of the problem it was still possible to arrive at a very reasonable agreement index (R_1 = 0.0832). Unit cell checks were performed on the Gd^{III} and Nd^{III} analogues (Table S2†), confirming these to be isostructural (see ESI†). Crystals of both **2** and **3** diffracted poorly relative to those of **1**, therefore only this analogue has been reported in full.

Magnetic measurements

Magnetic measurements were carried out on a Quantum Design MPMS SQUID magnetometer in direct current (dc) mode. Microcrystalline samples of **2** and **3** were separately compacted and immobilized into cylindrical PTFE sample holders. Experimental dc data were recorded at 0.1 T and 1.0 T in the temperature range 2.0–290 K, and isothermal curves up to 5 T in the range of 2–13 K. All data were corrected for the diamagnetic contributions of the sample holders and the complex. AC susceptibility data were also routinely collected at zero static bias field in the 2.0–50 K/3–1000 Hz range using an amplitude of B_{ac} = 3 G. However, no relevant out-of-phase signals were detected for both compounds. For the evaluation of the magnetocaloric effects of **3**, magnetic susceptibility data were collected on polycrystalline powders on a Quantum Design Dynacool PPMS equipped with a 9 T magnet in the temperature range 300–2 K. The samples were added to Quantum Design gelatin capsules with eicosane present and then transferred to a Quantum Design sample straw (AGC2). Diamagnetic corrections from the holders and eicosane were applied.

Heat capacity measurements

The heat capacity of **3** was measured by the relaxation method for temperatures down to 0.3 K and constant magnetic fields from 0 to 7 T, using a Quantum Design PPMS, equipped with a ^{3}He cryostat. The experiments were performed on a thin pressed pellet (*ca.* 1 mg) of a polycrystalline sample of **3**, thermalized by *ca.* 0.2 mg of Apiezon N grease, whose contribution was subtracted by using a phenomenological expression.

Results and discussion

Structure description

Complexes **1–3** were synthesized by reacting Ln^{III}_2, H_8TBC[8], NBu_4OH, and 1,3,5-tricarboxylic acid in 8 mL of DMF/MeOH/$CHCl_3$ (v : v : v = 3/3/2) under solvothermal conditions at 120 °C for 48 hours (**1** and **2**) or at 150 °C for 24 hours (**3**). We note that the syntheses require the presence of DMF. When conducted under an inert atmosphere, the syntheses produce the same title compounds but in lower yields. The block-like single crystals of La^{III}_{18} (**1**), Nd^{III}_{18} (**2**), and Gd^{III}_{18} (**3**) were isolated by either slow diffusion of hexane into a concentrated solution of the mother liquor containing the product (**1**, **2**), or by slow evaporation of the mother liquor (**3**), see Experimental section for full details. The crystals were all found to be in the trigonal crystal system and structure solution was performed in the space group $P\bar{3}1c$ (Tables S1 and S2†). The three complexes are structurally analogous, therefore we only provide a representative molecular structural description of **1**. The La^{III}_{18} skeleton is fully surrounded by TBC[8] units (Fig. 1). Internally, it is templated by a chloride anion (Fig. 2a) located in the center of the molecule (Cl–μ_3-OH: 3.47 Å), from which the closest twelve μ_3-OH^- ligands bind 'internally' to the eighteen La^{III} ions (La–O: 2.553(7), 2.574(6), and 2.590(6) Å). 'Externally' μ_3-Cl^- (La–Cl: 2.974(4) Å), μ_4-O^{2-} (La–O: 2.5533(5) and 2.8249(18) Å), and μ_3-CO_3^{2-} (La–O: 2.622(9) Å) ions and the fully deprotonated TBC[8] ligands (La–O: 2.404(9)–2.589(8) Å) connect the metallic core. The TBC[8] ligands are in a twofold double-cone conformation with O-atoms in each phenoxide unit displaying a μ_2-binding mode to the La ions (Fig. 1). The remaining coordination sites around the metal center are occupied by terminally bonded H_2O and DMF molecules. The OH counter anion is located at ~2.6 Å from the three equivalent coordinated water molecules (Fig. S3a†). Bond Valence Sum (BVS) calculations[12] (Table S4†) confirm the assignment of La^{III} ions, fully deprotonated TBC[8] ligands, and μ_3-OH^-/Cl^- ions. The cationic cluster is highly symmetric (D_{3h}, trigonal planar) with the C_3 axis passing through the two central carbon atoms of the two carbonate ligands (Fig. S3a†). La1, La2, and La3 in the asymmetric unit (Fig. 2c) adopt distorted square antiprismatic $Ln^{III}O_8$, distorted square antiprismatic $Ln^{III}O_6Cl_2$, and distorted capped square antiprismatic $Ln^{III}O_8Cl$ geometries, respectively (Fig. S1†).

Hydroxide-bridged lanthanide clusters are typically assembled by the repetition of small building blocks that construct the structural skeleton of the clusters. For example, Ln^{III}_{104} is formed by corner-sharing trigonal bipyramidal

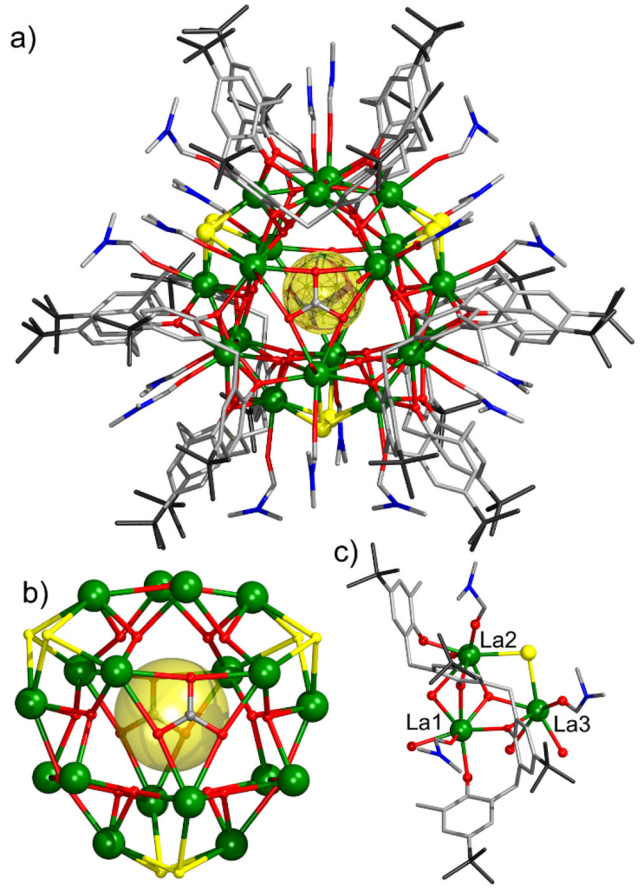

Fig. 2 (a) Molecular structure of $[La^{III}_{18}(TBC[8]\text{-}8H)_3(\mu_4\text{-}O)_3(\mu_3\text{-}Cl)_6(\mu_3\text{-}OH)_{12}(\mu_3\text{-}CO_3)_2(H_2O)_6(DMF)_{18}Cl]^+$. (b) The $[La^{III}_{18}(\mu_4\text{-}O)_3(\mu_3\text{-}Cl)_6(\mu_3\text{-}OH)_{12}(\mu_3\text{-}CO_3)_2]$ fragment showing the coordination modes of the OH/O/Cl/CO_3 ligands. (c) The asymmetric unit. Color code: Ln: green, O: red, N: blue, Cl: yellow, and C: gray. H atoms, solvent molecules, and OH counter anion are omitted for clarity.

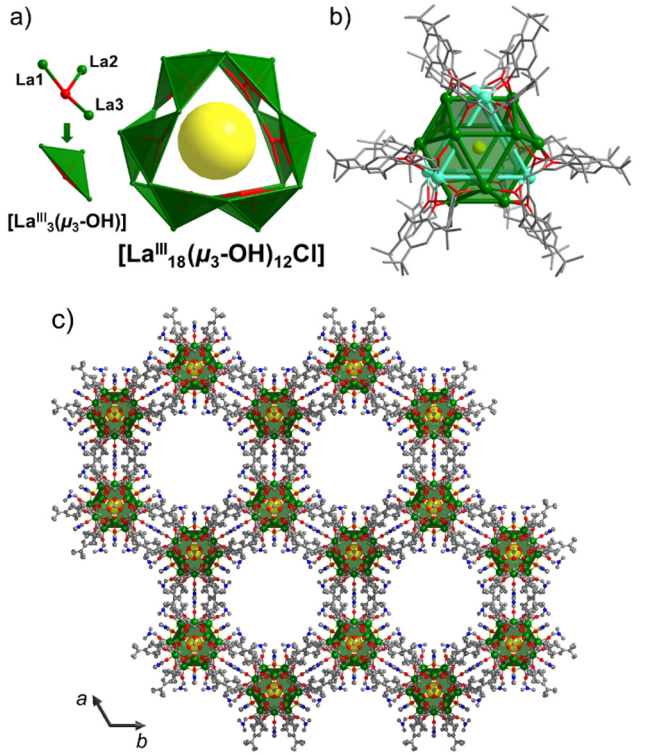

Fig. 3 (a) Vertex-sharing of triangular $\{Ln_3(\mu_3\text{-}OH)\}$ building blocks in the $[Ln^{III}_{18}(\mu_3\text{-}OH)_{12}Cl]$ fragment. (b) Polyhedral representation of the 18-metal-atoms core structure as an intercalated trigonal prism (cyan) and an irregular polyhedron (green). (c) Crystal packing of **1** viewed along the *c* axis exhibiting cylindrical channels with a diameter of ~22 Å. Color code as in Fig. 2. H atoms, solvent molecules, and OH counter anions are omitted for clarity.

$\{Ln_5(\mu_3\text{-}OH)_6\}$ units and Ln^{III}_{60} by vertex-sharing cubane-like $\{Ln_4(\mu_3\text{-}OH)_4\}$ moieties. The use of edge- or vertex-sharing triangular $\{La_3(\mu_3\text{-}OH)\}$ building blocks has been reported in the formation of small clusters with nuclearities ranging from four to twelve, due to the inexistence of templating anions. In this work, the use of H_8TBC[8] and templating chloride ion has enabled us to construct Ln^{III}_{18} *via* assembly of twelve vertex-sharing triangular $\{La_3(\mu_3\text{-}OH)\}$ motifs that build the metallic core (Fig. 3a). A polyhedral representation of the metallic skeleton (Fig. 3b) describes an intercalated trigonal prism and an irregular polyhedron that consists of six equilateral triangles and eight isosceles trapezia. It is important to note that the release of chloride and carbonate anions during the solvothermal reaction is essential for structuring the metallic skeleton. These anions are slowly produced *in situ* by the dehalogenation of chloroform and the decomposition of DMF, and/or fixation of atmospheric CO_2. The use of 1,3,5-tricarboxylic acid, although not integrated into the structure, is mandatory. We postulate that it may prevent the isolation of smaller TBC[8]-based Ln complexes, particularly those based on single- or double-deckers. Instead, it facilitates the formation of La^{III}_{18}, the first such structure supported by three TBC[8] ligands.

Analysis of the crystal packing reveals a mesoporous material, whose void space corresponds to ~50% of its volume (using a 1.5 Å spherical probe radius; Fig. S2†).[13] The crystal lattice exhibits cylindrical channels along the *c* axis with a diameter of ~22 Å created by the arrangement of La^{III}_{18} molecules in hexagonal motifs mediated by intermolecular $CCH_3(^tBu)$–$CCH_3(^tBu)$ contacts of ~3.9 Å (Fig. S3b†). The OH^- counter anion is H-bonded to the terminally bound water molecules of the cluster (La–OH_2···OH^-: 2.60 Å; Fig. S3†).

FT-IR, UV-Vis, and TGA–DSC experiments

In the FT-IR spectra of **1–3** (Fig. S4†), the most important bands are related to vibrations associated with ν(C–H) ~2953–2863 cm^{-1} ν(C═O) ~1653 cm^{-1} (vs) (characteristic of carbonate), ν(arC–C) ~1486 cm^{-1} (vs) (localized in the TBC[8] ligand; uncoordinated H_8TBC[8] ligand shows two smaller bands at 1486 and 1452 cm^{-1}), and ν(C–O) at ~1296 (m), ~1267 (m), and ~1206 cm^{-1} (s). The absence of the PhO–H vibration band, present in the uncoordinated H_8TBC[8] ligand at 1246 cm^{-1} is another proof of the deprotonation of the

ligand upon coordination. The electronic absorption spectra of **1–3** in $CHCl_3$ solutions display an intense absorption band at ~304 nm, attributed to π–π* electronic transitions centered on the aromatic rings of the fully deprotonated TBC[8] (Fig. S6†). Their electronic absorption curves are unchanged over a period of 24 hours in $CHCl_3$ solutions. The TGA curves of **1–3** (Fig. S7–S9†) show a slow release of crystallization solvent up to ~220 °C, wherefrom a rapid loss of mass occurs between 220 and 420 °C, corresponding with the decomposition of the structures. These two mass-loss steps are evidenced by a broad endothermic peak at ~380 °C by differential scanning calorimetry (DSC) in the three complexes. For complexes **1–3**, the experimental patterns closely mirror each other, as anticipated for isostructural analogs.

Magnetic studies

Direct current (dc) magnetic susceptibility and magnetization measurements of **2** and **3** are shown in Fig. 4. At 290 K, the $\chi_m T$ values of 25.3 (**2**) and 141.0 cm^3 K mol^{-1} (**3**) are within the anticipated range of 25–28 cm^3 K mol^{-1} and 137–142 cm^3 K mol^{-1} for eighteen non-interacting Nd^{III} and Gd^{III} centers, respectively.[14] Upon cooling, the $\chi_m T$ value of **2** progressively decreases to 9.7 (at 0.1 T) or 9.0 cm^3 K mol^{-1} (1.0 T) at 2 K. The $\chi_m T$ value of complex **3** remains constant between 300 and 50 K, wherefrom it rapidly decreases to 64.9 (0.1 T) or 59.1 cm^3 K mol^{-1} (1.0 T) at 2.0 K. The $\chi_m T$ *vs.* T data of **2** is caused by the thermal depopulation of the m_J energy sublevels of the predominant ground term ($^4I_{9/2}$) that results from the combined action of electron–electron repulsion and spin–orbit coupling in the Nd^{III} center, and the ligand field splitting the m_J sublevels. At lower temperatures (T < 10 K), the diverging $\chi_m T$ *vs.* T curves at 0.1 and 1 T can be attributed to the Zeeman effect and predominantly antiferromagnetic exchange interactions between the Nd^{III} centers. The almost isotropic nature of the

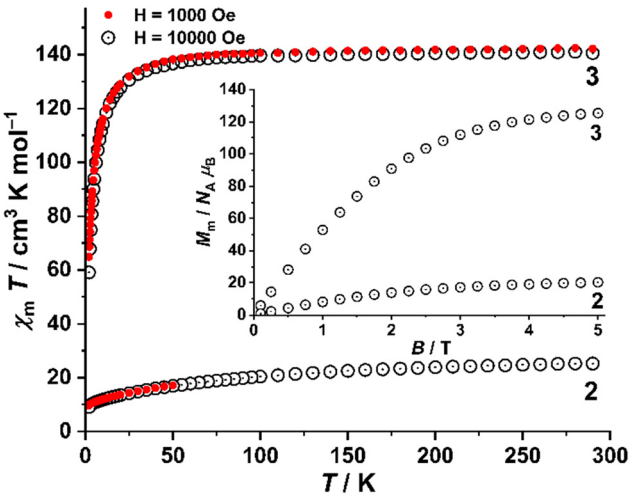

Fig. 4 Susceptibility data for **2** and **3** in static magnetic fields: $\chi_m T$ *vs.* T of **2** and **3** at 0.1 (filled red circles) and 1.0 T (open black circles). Inset: molar magnetization M_m *vs.* applied magnetic field B at 2.0 K.

Gd^{III} ion (s = 7/2, $^8S_{7/2}$) leads to a nearly constant $\chi_m T$ value at T > 100 K.

Due to the marginal splitting of the four doublet energy states of the $^8S_{7/2}$ ground term, the distinct drop of $\chi_m T$ at T < 50 K can only be attributed to the predominantly antiferromagnetic exchange interactions between the Gd^{III} centers. Fitting the χ_m data of **3** to the Curie–Weiss law yields the Weiss temperature θ = −3.1 K, denoting weak yet significant antiferromagnetic correlations, as also confirmed by heat capacity (c_p) measurements (Fig. S11†). The zero-field magnetic contribution to c_p can be well described by the Schottky model for eighteen spins s = 7/2 per cluster and an effective magnetic field B_{eff} = 0.6 T that mimics the magnetic interactions (notably, $g\mu_B s B_{eff}$ = 2.8 K ≈ $|\theta|$, for g = 2.0). Considering the isomorphous nature of **2** and **3**, it is highly probable that antiferromagnetic interactions also exist in **2**. At 2.0 K, the molar magnetization M_m *vs.* B plots of **2** and **3** show an approximately positive linear dependence and reach 20.2 (**2**) and 125.4 $N_A\mu_B$ (**3**), respectively, at 5.0 T (roughly 34% of the saturation value 58.9 $N_A\mu_B$ for **2**). This is due to the measurement of powdered samples, *i.e.*, the determination of the mean value of randomly oriented crystallites, and the additional contribution of magnetically anisotropic Nd^{III} centers in complex **2**. The magnetization data further confirm the presence of predominantly antiferromagnetic exchange interactions in both compounds.

The MCE of **3** was investigated by recording the isothermals (2–13 K) of the magnetization data in an applied field (Fig. S10†) and the heat capacity at a constant field between 0.3 and 30 K (Fig. S11†). Calculation of the temperature and field dependences of the magnetic entropy change from M_m data uses the Maxwell equation:

$$\Delta S_m(T, \Delta B) = \int_0^B \left(\frac{\partial M_m}{\partial T}\right)_B dB',$$

for any applied magnetic field change $\Delta B = B - 0$.[5,15,16] The c_p data provide better information in terms of the MCE since they allow us to determine both $\Delta S_m(T,\Delta B)$ and $\Delta T_{ad}(T,\Delta B)$ changes, straightforwardly from the entropy (Fig. S10†), calculated as:

$$S(T, B) = \int_0^T \frac{c_p}{T'} dT'.$$

The corresponding changes of ΔS_m and ΔT_{ad} at different T and ΔB are shown in Fig. 5. Both approaches, based on calculating ΔS_m from M_m and c_p data, respectively, provide identical results. We find that both $-\Delta S_m$ and ΔT_{ad} improve gradually by increasing ΔB, reaching the values of 23.7 J K^{-1} kg^{-1} and 8.6 K, respectively, at 2.2 K and ΔB = 7 T. The maximum experimental entropy change corresponds to *ca.* 77% of the available entropy content, *i.e.*, 18 × $R_s$ln(2s + 1) = 30.8 J K^{-1} kg^{-1} (R_s = R/M). The MCE is surprisingly high considering the supramolecular nature of the TBC[8] ligand – with its low magnetic density given by M_w/N_{Gd}, where M_w is the molecular weight and N_{Gd} is the number of gadolinium metal ions constituting

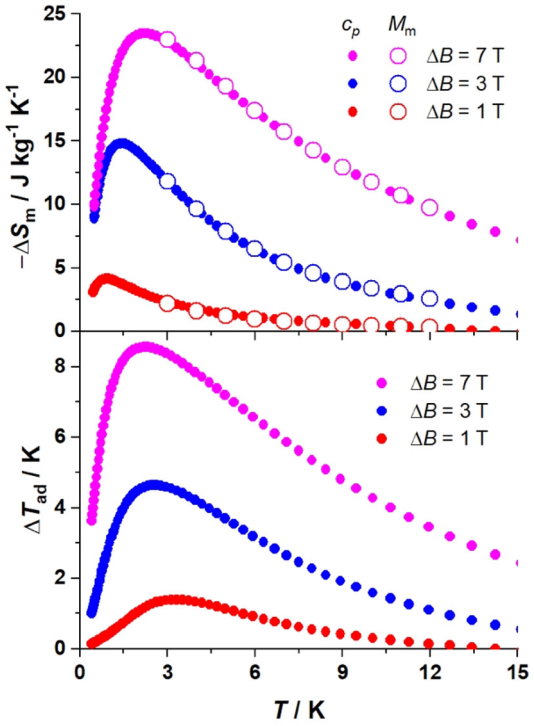

Fig. 5 Magnetic entropy change (top) and adiabatic temperature change (bottom) for **3**, obtained from the molar magnetization (open symbols) and heat capacity (filled symbols) data, shown in Fig. S10 and S11,† respectively, for selected applied field changes, as labeled.

the cluster. Although the magnetocaloric response of **3** is not in close range to the best molecular magnetorefrigerants based on polynuclear homometallic lanthanide clusters,[1a,b,2a,16] it represents the best result obtained with calix[*n*]arene-based molecular clusters.[17]

Conclusions

In summary, the use of the "anion template strategy" and the involvement of "templating ligands" – hitherto neglected in calix[*n*]arene coordination chemistry – allowed us to synthesize a family of highly symmetric (D_{3h}, trigonal planar) Ln^{III}_{18} coordination clusters. The title compounds exhibit structural features common to high-nuclearity homometallic lanthanide hydroxy clusters obtained with smaller ligands (*e.g.*, Gd^{III}_{140}, Ln^{III}_{104}, Dy^{III}_{76}) but uncommon in calix[*n*]arene-based clusters, such as high symmetry, the presence of templating anions, and the presence of an inner core constructed by the repetition of small $\{Ln_x(\mu_n\text{-}OH)_y\}$ building blocks. The crystal packing of the molecules creates a material with cylindrical channels of ~22 Å diameter along the *c* axis of the unit cell. Based on the size of the solvent channels, the title compounds could be of interest for the development of materials for sorption experiments. Investigation of the magnetocaloric effect on the gadolinium derivative yields a $-\Delta S_m$ = 23.7 J K^{-1} kg^{-1}; this value shows the potential of engineering magnetic refrigerants with calix[*n*]arene ligands. Current work focuses on (a) the synthesis of Gd^{III}_{18} analogs with C[8] (*i.e.*, exchanging ^{t}Bu groups in the ligand to hydrogens) to increase the magnetic density (M_w/N_{Gd}) and thus the magnetic entropy content, and (b) the application of the reported strategies targeting larger homometallic lanthanide clusters. Results stemming from the ongoing work will be communicated in due course and may lead to a better understanding of the mechanism involved in the construction of high-nuclearity lanthanide clusters with TBC[8] and the relationship between structural modifications and magnetic entropy changes.

Conflicts of interest

There are no conflicts to declare.

Acknowledgements

Yushu Jiao gratefully acknowledges financial support from the Chinese Scholarship Council (CSC). This work was supported by MICINN (PID2021-124734OB-C21). David Gracia acknowledges financial support from the Aragón regional government through a doctoral fellowship. Angelos Canaj thanks The Leverhulme Trust (grant RPG-2021-176).

References

1 (*a*) X.-Y. Zheng, Y.-H. Jiang, G.-L. Zhuang, D.-P. Liu, H.-G. Liao, X.-J. Kong, L.-S. Long and L.-S. Zheng, *J. Am. Chem. Soc.*, 2017, **139**, 18178; (*b*) J.-B. Peng, X.-J. Kong, Q.-C. Zhang, M. Orendáč, J. Prokleška, Y.-P. Ren, L.-S. Long, Z. Zheng and L.-S. Zheng, *J. Am. Chem. Soc.*, 2014, **136**, 17938; (*c*) X.-Y. Li, H.-F. Su, Q.-W. Li, R. Feng, H.-Y. Bai, H.-Y. Chen, J. Xu and X.-H. Bu, *Angew. Chem., Int. Ed.*, 2019, **58**, 10184; (*d*) L. Qin, Y.-Z. Yu, P.-Q. Liao, W. Xue, Z. Zheng, X.-M. Chen and Y.-Z. Zheng, *Adv. Mater.*, 2016, **28**, 10772–10779; (*e*) Z.-R. Luo, H.-L. Wang, Z.-H. Zhu, T. Liu, X.-F. Ma, H.-F. Wang, H.-H. Zou and F.-P. Liang, *Commun. Chem.*, 2020, **3**, 1; (*f*) X. M. Luo, Z. B. Hu, Q. F. Lin, W. Cheng, J. P. Cao, C. H. Cui, H. Mei, Y. Song and Y. Xu, *J. Am. Chem. Soc.*, 2018, **140**, 11219; (*g*) M. Wu, F. Jiang, D. Yuan, J. Pang, J. Qian, S. A. Al-Thabaiti and M. Hong, *Chem. Commun.*, 2014, **50**, 1113; (*h*) X.-Y. Zheng, X.-J. Kong, Z. Zheng, L.-S. Long and L.-S. Zheng, *Acc. Chem. Res.*, 2018, **51**, 517; (*i*) J. Dong, P. Cui, P.-F. Shi, P. Cheng and B. Zhao, *J. Am. Chem. Soc.*, 2015, **137**, 15988; (*j*) N.-F. Li, X.-M. Luo, J. Wang, J.-L. Wang, H. Mei, Y. Song and Y. Xu, *Sci. China: Chem.*, 2022, **65**, 1577.

2 (*a*) F.-S. Guo, Y.-C. Chen, L.-L. Mao, W.-Q. Lin, J.-D. Leng, R. Tarasenko, M. Orendáč, J. Prokleška, V. Sechovský and M.-L. Tong, *Chem. – Eur. J.*, 2013, **19**, 14876; (*b*) X.-Y. Li, Y. Jing, J. Zheng, H. Ding, Q. Li, M.-H. Yu and X.-H. Bu, *Cryst. Growth Des.*, 2020, **20**, 5294.

3 X.-Y. Zheng, J. Xie, X.-J. Kong, L.-S. Long and L.-S. Zheng, *Coord. Chem. Rev.*, 2019, **378**, 222.

4 (*a*) K. Su, F. Jiang, J. Qian, J. Pang, F. Hu, S. M. Bawaked, M. Mokhtar, S. A. Al-Thabaiti and M. Hong, *Inorg. Chem. Commun.*, 2015, **54**, 34; (*b*) S. M. Taylor, S. Sanz, R. D. McIntosh, C. M. Beavers, S. J. Teat, E. K. Brechin and S. J. Dalgarno, *Chem. – Eur. J.*, 2012, **18**, 16014.

5 E. K. Brechin and M. Evangelisti, *Dalton Trans.*, 2010, **39**, 4672.

6 (*a*) J.-J. Hu, Y. Peng, S.-J. Liu and H.-R. Wen, *Dalton Trans.*, 2021, **50**, 15473; (*b*) S.-J. Liu, S.-D. Han, J.-P. Zhao, J. Xu and X.-H. Bu, *Coord. Chem. Rev.*, 2019, **394**, 39; (*c*) J.-L. Liu, Y.-C. Chen, F.-S. Guo and M.-L. Tong, *Coord. Chem. Rev.*, 2014, **281**, 26; (*d*) P. Konieczny, W. Sas, D. Czernia, A. Pacanowska, M. Fitta and R. Pełka, *Dalton Trans.*, 2022, **51**, 12762; (*e*) T. N. Hooper, J. Schnack, S. Piligkos, M. Evangelisti and E. K. Brechin, *Angew. Chem., Int. Ed.*, 2012, **51**, 4633; (*f*) T. G. Tziotzi, D. Gracia, S. J. Dalgarno, J. Schnack, M. Evangelisti, E. K. Brechin and C. J. Milios, *J. Am. Chem. Soc.*, 2023, **145**, 7743.

7 See, *e.g.*: S. R. Bare, M. Lilly, J. Chermak, R. Eggert, W. Halperin, S. Hannahs, S. Hayes, M. Hendrich, A. Hurd, M. Osofsky and C. Tway, "Responding to the U.S. Research Community's Liquid Helium Crisis",DOI: **10.7936/K7571B6D**, Oct. 2016.

8 (*a*) A. E. Dearle, D. J. Cutler, H. W. L. Fraser, S. Sanz, E. Lee, S. Dey, I. F. Diaz-Ortega, G. S. Nichol, H. Nojiri, M. Evangelisti, G. Rajaraman, J. Schnack, L. Cronin and E. K. Brechin, *Angew. Chem., Int. Ed.*, 2019, **58**, 16903; (*b*) A. E. Dearle, D. J. Cutler, M. Coletta, E. Lee, S. Dey, S. Sanz, H. W. L. Fraser, G. S. Nichol, G. Rajaraman, J. Schnack, L. Cronin and E. K. Brechin, *Chem. Commun.*, 2022, **58**, 52.

9 B. M. Furphy, J. M. Harrowfield, D. L. Kepert, B. W. Skelton, A. H. White and F. R. Wilner, *Inorg. Chem.*, 1987, **26**, 4231–4236.

10 O. V. Dolomanov, L. J. Bourhis, R. J. Gildea, J. A. K. Howard and H. Puschmann, *J. Appl. Crystallogr.*, 2009, **42**, 339–341.

11 G. M. Sheldrick, *Acta Crystallogr., Sect. A: Found. Adv.*, 2015, **71**, 3–8.

12 (*a*) I. D. Brown and D. Altermatt, *Acta Crystallogr., Sect. B: Struct. Sci.*, 1985, **41**, 244; (*b*) K. Knížek, *Kalvados software for calculation of BVS*. **https://www.fzu.cz/~knizek/kalvados/index.html**.

13 Calculation by using the void calculation tool in Mercury 2022.3.0 programme for a spherical probe radius of 1.5 Å and a grid spacing of 0.3 Å.

14 H. Lueken, *Magnetochemie*, Teubner Verlag, Stuttgart, 1999.

15 See, *e.g.*: (*a*) S.-D. Han, X.-H. Miao, S.-J. Liu and X.-H. Bu, *Inorg. Chem. Front.*, 2014, **1**, 549; (*b*) F. Danker, C. Anderer, M. Poschmann, H. Terraschke, C. Näther, J. van Leusen, W. Bensch and P. Kögerler, *Eur. J. Inorg. Chem.*, 2020, 1751; (*c*) B. G. Shen, J. R. Sun, F. X. Hu, H. W. Zhang and Z. H. Cheng, *Adv. Mater.*, 2009, **21**, 4545.

16 (*a*) Y. Zhou, X. Zheng, J. Cai, Z. Hong, Z. Yan, X. Kong, Y. Ren, L. Long and L. Zheng, *Inorg. Chem.*, 2017, **56**, 2037; (*b*) M. Wu, F. Jiang, X. Kong, D. Yuan, L. Long, S. A. Al-Thabaitic and M. Hong, *Chem. Sci.*, 2013, **4**, 3104; (*c*) X. Zheng, J. Peng, X. Kong, L. Long and L. Zheng, *Inorg. Chem. Front.*, 2016, **3**, 320; (*d*) L. Chang, G. Xiong, L. Wang, P. Cheng and B. Zhao, *Chem. Commun.*, 2013, **49**, 1055; (*e*) S. Han, X. H. Miao, S. J. Liu and X. H. Bu, *Inorg. Chem. Front.*, 2014, **1**, 549.

17 (*a*) G. Karotsis, S. Kennedy, S. J. Teat, C. M. Beavers, D. A. Fowler, J. J. Morales, M. Evangelisti, S. J. Dalgarno and E. K. Brechin, *J. Am. Chem. Soc.*, 2010, **132**, 12983; (*b*) G. Karotsis, M. Evangelisti, S. J. Dalgarno and E. K. Brechin, *Angew. Chem., Int. Ed.*, 2009, **48**, 9928.